Metabolic adaptations in models of fatty liver disease

Hijmans, Brenda

Appendices

Appendix A

Taqman qPCR primer and probe sequences.

Table A.1: Taqman qPCR primer and probe sequences.

gene	forward primer 5'-3'	reverse primer 5'-3'	probe 5'-3'
18S	CGGCTACCACATCCAAGGA	CCAATTACAGGCCTCGAAA	CGCGCAAATTACTCCCGA
36b4	GCTTCATTGTGGGAGCAGACA	CATGGTGTTCTTGCCCATCAG	TCCAAGCAGATGCAGCAGATCCGC
Abcg1	CAAGACCCTTTTGAAAGGGATCTC	GCCAGAATATTCATGAGTGTGGAC	CCCATGATGGCCACCAGCTCTCC
Abcg5	TCAGGACCCCAAGGTCATGAT	AGGCTGGTGGATGGTGACAAT	CCACAGGACTGGACTGCATGACTGCA
Acaca	GCCATTGGTATTGGGGCTTAC	CCCGACCAAGGACTTTGTTG	CTCAACCTGGATGGTTCTTTGTCCCAGC
Acox1	GCCACGGAACTCATCTTCGA	CCAGGCCACCACTTAATGGA	CCACTGCCACATATGACCCCAAGACCC
Acsl3	GCCAACGTGGAAAAGAAAGC	GTGGACCCACTTGTGTACATGATT	AGCAAACCACTGCCCTCAGATATTGCA
Agl	CTATCCCGCTCGGGTAACT	AGAGTTCGAATCCTCCAGAAGCCA	GCTTCTCCATCTCGTTCAGTAG
Angptl4	AGATCCAGCAATTGTTCCAGAAG	AAGAGGTCTATCTGGCTCTGAAGATT	CCCAGCAGCAGAGATACCTATCAAAGCAG
Ap2	GATCACCATTAAATCTGAAAGTACCTTTA	GGTTATGGTGCTCTTGACTTTCC	ACTGAGATTTCCTTCATACTGGGCCAGGA
Apob	GCCCATTGTGGACAAGTTGATC	CCAGGACTTGGAGGTCTTGGA	AAGCCAGGGCCTATCTCCGCATCC
ApoC1	GGGCAGCCATTGAACATATCA	TTGCCAAATGCCTCTGAGAAC	CCCGGGTCTTGGTCAAAATTTCCTTC
Apoc2	TTACTGGACCTCTGCCAAGGA	CCCTGAGTTTCTCATCCATGC	CCAAAGACCTGTACCAGAAGACATACCCGA
Apoc3	CCAAGACGGTCCAGGATGC	ACTTGCTCCAGTAGCCTTTCAGG	CCATCCAGCCCCTGGCCACC
ApoE	CCTGAACCGCTTCTGGGATT	GCTCTTCCTGGACCTGGTCA	AAAGCGTCTGCACCCAGCGCAGG
Cd36	GATCGGAACTGTGGGCTCAT	GGTTCCTTCTTCAAGGACAACTTC	AGAATGCCTCCAAACACAGCCAGGAC
Chrebpα	CGACACTCACCCACCTCTTC	TTGTTCAGCCGGATCTTGTC	CCTGGCTTACAGTGGCAAGCTGGTCTCT
Chrebpβ	TCTGCAGATCGCGTGGAG	CTTGTCCCGGCATAGCAAC	CTCAGTGGCAAGCTGGTCTCTCCCA
Cyp7a1	CAGGGAGATGCTCTGTGTTCA	AGGCATACATCCCTTCCGTGA	TGCAAAACCTCCAATCTGTCATGAGACCTCC
Elvol5	TGGCTGTTCTTCCAGATTGGA	CCCTTTCTTGTTGTAAGTCTGAATGTA	CATGATTTCCCTGATTGCTCTCTTCACAAAC
Elvol6	ACACGTAGCGACTCCGAAGAT	AGCGCAGAAAACAGGAAAGACT	TTTCCTGCATCCATTGGATGGCTTC
Fabp1	GAACTTCTCCGGCAAGTACCAA	TGTCCTTCCCTTTCTGGATGAG	CCATTCATGAAGGCAATAGGTCTGCCC
Fabp4	GATCACCATTAAATCTGAAAGTACCTTTA	GGTTATGGTGCTCTTGACTTTCC	ACTGAGATTTCCTTCATACTGGGCCAGGA
Fasn	GGCATCATTGGGCACTCCTT	GCTGCAAGCACAGCCTCTCT	CCATCTGCATAGCCACAGGCAACCTC
Fgf21	CCGCAGTCCAGAAAGTCTCC	TGACACCCAGGATTTGAATGAC	CCTGGCTTCAAGGCTTTGAGCTCCA
*Gaa**	CTTCAAGATCAAAGATCCTGCTAGTAAG	TGAGAATTCCACGCTGTAAAGTG	
*Gabarapl1**	ACGCCTTATTCTTCTTTGTCAACA	CCTCGTGGTTGTCCTCATACAG	
Gbe1	CCCCTTTCACTCCAGTAATTGATC	GCCCAAACTCATTACCCATGA	ATGATTCGTCTCATCACTCACGGGCTC
Gck	CCTGGGCTTCACCTTCTCCTT	GAGGCCTTGAAGCCCTTGGT	CACGAAGACATAGACAAGGGCATCCTGCTC
Gkrp	TGGGACCATGCCAAGCA	TTCATACCCTGACAACTCCCATT	CAGCATGTGATCGAGACCCCTGAGC
Gs	GCTCTCCAGACGATTCTTGCA	GTGCGGTTCCTCTGAATGATC	CCTCTACGGGTTTTGTAAACAGTCACGCC
Gp	GAAGGAGGCAAACGGATCAAC	TCACGATGTCCGAGTGGATCT	CCTCTGCATCGTGGGCTGCCA
Gpat	GCTATCATGTCCACCCACATTG	ACTTCCTCCTTCATCACAAAGAAGTC	CTCCTCTACAGACACAGGCAGGGAATCC
Hmgcr	CCGGCAACAACAAGATCTGTG	ATGTACAGGATGGCGATGCA	TGTCGCTGCTCAGCACGTCCTCTTC
Hmgcs	CGATGGTGTAGATGCTGGAAAG	CTCCATCAGTTTCTGAACCACAGT	CGATCCGTGCAGAAGCCCATCC
Hsl	GAGGCCTTTGAGATGCCACT	AGATGAGCCTGGCTAGCACAG	CCATCTCACCTCCCTTGGCACACAC
Lcad	TACGGCACAAAAGAACAGATCG	CAGGCTCTGTCATGGCTATGG	CACTTGCCCGCCGTCATCTGG
Ldlr	GCATCAGCTTGGACAAGGTGT	GGGAACAGCCACCATTGTTG	CACTCCTTGATGGGCTCATCCGACC
Lpl	AAGGTCAGAGCCAAGAGAAGCA	CCAGAAAAGTGAATCTTGACTTGGT	CCTGAAGACTCGCTCTCAGATGCCCTACA
Lrp1	TCAGACGAGCCTCCAGACTGT	ACAGATGAAGGCAGGGTTGGT	CCAGTTCCAGTGCTCCACCGGC

Full gene names are explained throughout the manuscript. *SYBR green method used. – *Continued on next page.*

Table A.1 – *continued from previous page*

gene	forward primer 5'-3'	reverse primer 5'-3'	probe 5'-3'
Lxrα)	TGCCTGATGTTTCTCCTGATTCT	CCTCCCTGGTCTCCTGCAT	TTGAGGTTCTGTCTTCCACAACTCCGTTG
Me1	AGGCAGCGTCTTCCAAATATG	TCGATACTTGTTCAGGAGACGAA	TGGCAAAATCTTCAAACTGAATAAGGCAATTC
Mttp	CAAGCTCACGTACTCCACTGAAG	TCATCATCACCATCAGGATTCCT	ACCGCAAGACAGCGTGGGCTACA
Pparγ1	AACAAGACTACCCTTTACTGAAATTACCA	CACAGAGCTGATTCCGAAGTTG	ACACAGAGATGCCATTCTGGCCCAC
Pparγ2	CTATGAGCACTTCACAAGAAATTACCA	CACAGAGCTGATTCCGAAGTTG	ACACAGAGATGCCATTCTGGCCCAC
Plin	AGAACGTGCTCAGAGAGGTTACAG	GTGTTCTGCACGGTGTGTACC	CCTGCCCAACCCGAGAGGCC
Pltp	TTCCTCCTCAACCAGCAGATCT	CAGGAGGGAGTTGAGCAACAC	CCCTGTGCTCTACCATGCTGGGACG
Scd1	ATGCTCCAAGAGATCTCCAGTTCT	CTTCACCTTCTCTCGTTCATTTCC	CCACCACCACCATCACTGCACCTC
Srebpf1	GGAGCCATGGATTGCACATT	CCTGTCTCACCCCCAGCATA	CAGCTCATCAACAACCAAGACAGTGACTTCC
Srebpf2	CTGCAGCCTCAAGTGCAAAG	CAGTGTGCCATTGGCTGTCT	CCATCCAGCAGCAGGTGCAGACG
Sqs	TGGCGGTTCACTGAGAGCA	ATCACTGTTTGATATTTCTCAGCCAA	ACTTCCCCCACGATCTCCCTGGAGTTT
Ucp2	CGAAGCCTACAAGACCATTGC	ACCAGCTCAGCACAGTTGACA	CAGAGGCCCCGGATCCCTTCC
Vldlr	CCACAGCAGTATCAGAAGTCAGTGT	CACCTACTGCTGCCATCACTAAGA	CAGCTGCCTGGGCCATCCTTCC

Appendix B

ADAPT methodology

In this dissertation, the mathematical model that is used with ADAPT is composed of three compartments representing the liver, blood plasma, and peripheral tissues. The liver compartment includes reactions comprising the production, utilization and storage of triglyceride (TG) and cholesterol, and the mobilization of these metabolites to the endoplasmic reticulum (ER), where they are incorporated into nascent very low density lipoprotein (VLDL) particles. The VLDL particles are secreted in the plasma compartment where they serve as nutrients for peripheral tissues. Remnant particles are taken up and cleared by the liver. The model furthermore includes the hepatic uptake of free fatty acids (FFA) as well as high density lipoprotein (HDL) mediated reverse cholesterol transport (Figure B.1).

ADAPT is based on a time-dependent evolution of model parameters. The progression of adaptations is predicted by identifying necessary dynamic changes in the model parameters to describe the transition between experimental data obtained at different time-points. Subsequently, ADAPT provides trajectories of time-dependent changes in metabolic states, parameters, and fluxes, that occurred during the treatment intervention. In the following sections a step-by-step generic description of the methodology underlying ADAPT is presented.

Step 1: Calculating data interpolants.
Quantitative experimental data at different stages of a treatment intervention are required to study the dynamics of induced molecular adaptations. Data on hepatic TG, free cholesterol, and cholesterylester (CE) levels; fractional contributions of *de novo* lipogenesis to the hepatic TG pool; plasma concentrations of TG, total cholesterol, HDL cholesterol, FFA; VLDL-TG production rates, VLDL-TG catabolism rates, VLDL particle size, and VLDL composition obtained in C57BL/6J mice treated with T0901317 for 0, 1, 2, 4, 7, 14, and 21 days was used as input for ADAPT. Moreover, quantitative data on hepatic

cholesterol uptake and the deposition and synthesis of hepatic TG in cytoplasmic and microsomal fractions [387] in untreated control mice was derived from literature [388] and included in ADAPT.

To allow for estimation of dynamic trajectories of metabolic parameters and fluxes, continuous dynamic descriptions of the experimental data were used as input for ADAPT. For this purpose, cubic smoothing splines were calculated that describe the dynamic trend of the experimental data. To account for experimental and biological uncertainties a collection of splines was calculated using a Monte Carlo approach. Different random samples of the experimental data were generated assuming Gaussian distributions with means and standard deviations of the data. Subsequently, for each generated sample a cubic smoothing spline was calculated.

Step 2: Construction of a mathematical model.
A mathematical multi-compartment model was used describing TG and cholesterol metabolism. The mathematical model contains three compartments representing the liver, blood plasma, and periphery (Figure B.1). The liver includes the production, utilization and storage of TG and cholesterol, as well as the mobilization of these metabolites to the ER where they are incorporated into nascent VLDL particles. These VLDL particles are subsequently secreted in the plasma compartment and provide nutrients for peripheral tissues. The model furthermore includes the hepatic uptake of FFA from the plasma that predominantly originate from adipose tissue. Finally, the model includes the reverse cholesterol transport pathway, i.e., the net transport of cholesterol from peripheral tissues back to the liver via HDL.

The mathematical model contains 11 metabolic species (Table B.1) interlinked by 29 flux interactions (Table B.2). The flux equations (Table B.2) are based on mass-action kinetics. The ordinary differential equations are given by:

$$\frac{d[x_1]}{dt} = f_1 + f_4 + f_6 - f_2 - f_3 - f_5$$
$$\frac{d[x_2]}{dt} = f_3 - f_4 + V_{plasma}(f_{17} + f_{21})$$
$$\frac{d[x_3]}{dt} = f_5 - f_6 - f_{15}$$
$$\frac{d[x_4]}{dt} = f_9 - f_8 - f_{11} + V_{plasma}(\frac{f_{12}}{3} + f_{16} + f_{22})$$
$$\frac{d[x_5]}{dt} = f_{11} - f_9 - f_{28}$$

$$\frac{d[x_6]}{dt} = f_7 + f_{26} - f_{25} - f_{27}$$
$$\frac{d[x_7]}{dt} = f_{10} + f_{27} - f_{29} - f_{26}$$
$$\frac{d[x_8]}{dt} = \frac{f_{14}}{\mathrm{V_{plasma}}} - f_{16} - f_{18} - f_{22} - f_{23}$$
$$\frac{d[x_9]}{dt} = \frac{f_{15}}{\mathrm{V_{plasma}}} - f_{17} - f_{19}$$
$$\frac{d[x_{10}]}{dt} = f_{20} - f_{21}$$
$$\frac{d[x_{11}]}{dt} = f_{13} - f_{12}$$

The square brackets indicate the concentration of a specific metabolite. The blood plasma volume, given by $\mathrm{V_{plasma}}$, was assumed to be 1 mL [389].

Table B.1: Overview and description of the state variables included in the mathematical model.

State	Description
$\mathrm{x_1}$	Hepatic free cholesterol
$\mathrm{x_2}$	Hepatic CE (cytoplasm)
$\mathrm{x_3}$	Hepatic CE (ER)
$\mathrm{x_4}$	Hepatic TG (cytoplasm)
$\mathrm{x_5}$	Hepatic TG (ER)
$\mathrm{x_6}$	Hepatic *de novo* TG (cytoplasm)
$\mathrm{x_7}$	Hepatic *de novo* TG (ER)
$\mathrm{x_8}$	Plasma VLDL-TG
$\mathrm{x_9}$	Plasma VLDL-cholesterol
$\mathrm{x_{10}}$	Plasma HDL-cholesterol
$\mathrm{x_{11}}$	Plasma FFA

Step 3: Calibrating the model to the untreated phenotype.
In ADAPT the mathematical model is first used to describe the untreated phenotype. It is assumed that prior to the onset of a treatment intervention the concentrations and fluxes in the biological system are in a steady-state. The following protocol was employed to capture multiple parameter sets describing the untreated phenotype. The model parameters were estimated by applying a least squares algorithm that minimizes the sum of squared errors between the experimental data of the untreated phenotype and corresponding model outputs. The optimization procedure was repeated for all data interpolants

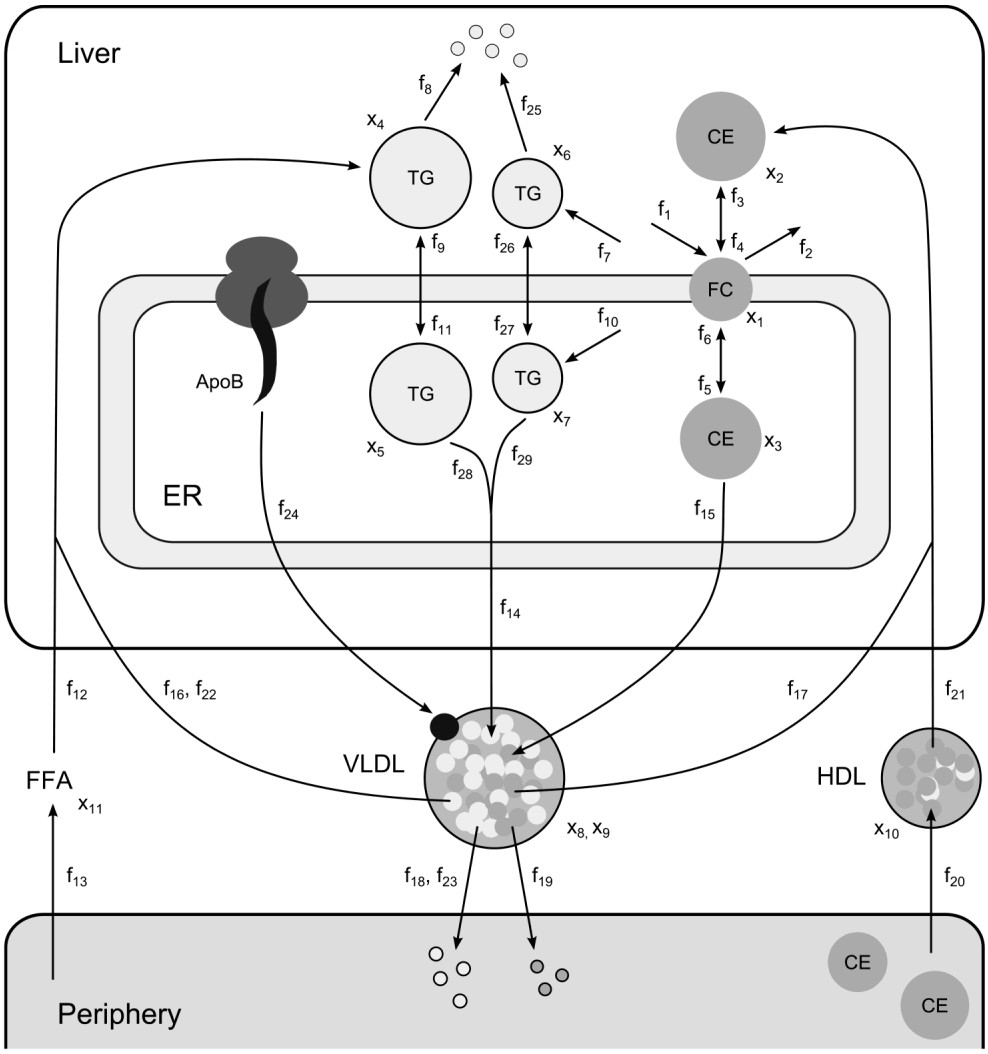

Figure B.1: Computational model of hepatic lipid and plasma lipoprotein metabolism. ApoB, apolipoprotein B; CE, cholesterylester; ER, endoplasmic reticulum; FFA, free fatty acids; FC, free cholesterol; HDL, high density lipoprotein; TG, triglyceride; VLDL, very low density lipoprotein. *See text for details.*

Table B.2: Overview and description of the fluxes included in the mathematical model.

Flux	Equation	Description
f_1	p_1	Hepatic *de novo* synthesis of free cholesterol
f_2	$p_2[x_1]$	Net hepatic catabolism of free cholesterol
f_3	$p_3[x_1]$	Hepatic synthesis of CE (cytoplasm)
f_4	$p_4[x_2]$	Hepatic conversion of CE (cytoplasm) to free cholesterol
f_5	$p_5[x_1]$	Hepatic synthesis of CE (ER)
f_6	$p_6[x_3]$	Hepatic conversion of CE (ER) to free cholesterol
f_7	p_7	Hepatic *de novo* synthesis of TG (cytoplasm)
f_8	$p_8[x_4]$	Hepatic catabolism of TG (cytoplasm)
f_9	$p_9[x_5]$	Hepatic transport of TG from the ER to the cytoplasm
f_{10}	p_{10}	Hepatic *de novo* synthesis of TG (ER)
f_{11}	$p_{11}[x_4]$	Hepatic transport of TG from the cytoplasm to the ER
f_{12}	$p_{12}[x_{11}]$	Hepatic uptake of FFA
f_{13}	p_{13}	Net efflux of FFA from peripheral tissues to plasma
f_{14}	$p_{14}([x_5]+[x_7])$	Hepatic secretion rate of VLDL-TG
f_{15}	$p_{15}[x_3]$	Hepatic secretion rate of VLDL-cholesterol
f_{16}	$p_{16}[x_8]$	Hepatic uptake of TG via whole-particle uptake
f_{17}	$p_{16}[x_9]$	Hepatic uptake of cholesterol via whole-particle uptake
f_{18}	$p_{17}[x_8]$	Peripheral uptake of TG via whole-particle uptake
f_{19}	$p_{17}[x_9]$	Peripheral uptake of cholesterol via whole-particle uptake
f_{20}	p_{20}	Peripheral efflux of cholesterol to HDL particles
f_{21}	$p_{21}[x_{10}]$	Hepatic uptake of HDL-cholesterol
f_{22}	$p_{18}[x_8]$	Hepatic uptake of TG via lipolytic enzymes
f_{23}	$p_{19}[x_8]$	Peripheral uptake of TG via lipolytic enzymes
f_{24}	p_{22}	Hepatic secretion rate of apolipoprotein B
f_{24}	p_{22}	Hepatic secretion rate of apolipoprotein B
f_{25}	$p_8[x_6]$	Hepatic catabolism of *de novo* TG (cytoplasm)
f_{26}	$p_9[x_7]$	Hepatic transport of *de novo* TG from the ER to the cytoplasm
f_{27}	$p_{11}[x_6]$	Hepatic transport of *de novo* TG from the cytoplasm to the ER
f_{28}	$p_{14}[x_5]$	Hepatic secretion rate of non *de novo* VLDL-TG
f_{29}	$p_{14}[x_7]$	Hepatic secretion rate of *de novo* VLDL-TG

calculated in step 1, resulting in a collection of parameter sets that describe the untreated phenotype. These parameter sets will serve as a starting point from which necessary dynamic changes are identified to describe the transition between experimental data obtained during different stages of the treatment.

Step 4: Estimating time-dependent changes of the model parameters.
Dynamic adaptations in metabolic processes are identified by inferring ne-

cessary dynamic changes in the model parameters which are therefore time-dependent. To this end, a simulation of the full treatment period was divided into a number of steps. First, the simulation is started using the parameters and model outputs of the untreated phenotype. Next, each subsequent step n, the system is simu-lated for a short time-period using the parameters and model outputs of the previous step n-1 as a starting point. The parameters at step n are re-estimated by minimizing the difference between the data interpolants and corresponding model outputs at step n. The optimization procedure is repeated for all para-meter set of the untreated phenotype, obtained in step 3.

Integration of gene expression data in ADAPT

To integrate information about the transcriptome into ADAPT, the optimization problem presented in step 4 was extended as follows. Time-course data of relative gene expression levels (Figure B.2) were used to constrain the dynamics of parameter trajectories. First, each step, parameter adaptations are preferred such that resulting parameter trajectories and corresponding gene expression profiles display temporal correlation, compared to uncorrelated scenarios. This was effectuated by including an additional objective function that maximizes the temporal correlation (Pearson correlation coefficient) between these profiles.

Secondly, gene expression data was also used to constrain the magnitude of dynamic variations in the parameter trajectories. It was assumed that parameters are less likely to change when corresponding gene expression levels (Table B.3) remain unchanged, compared to scenarios when expression of the genes is induced or repressed. Therefore, in latter cases parameter adaptations will be less penalized compared to former cases. This was effectuated by including an additional objective function that utilizes the time derivative of gene expression profiles to penalize parameter fluctuations. The higher the derivative, the lower the penalty will be.

An extra objective function that utilizes the time derivative of gene expression profiles to constrain parameter fluctuations was included. Parameter trajectories were estimated using 200 time steps. A collection of 20000 parameter trajectory sets was obtained that describe the experimental data. For the ADAPT analyses presented in chapter 2 and 3 we used 1000 parameter trajectory sets that displayed the highest temporal correlation with gene expression profiles.

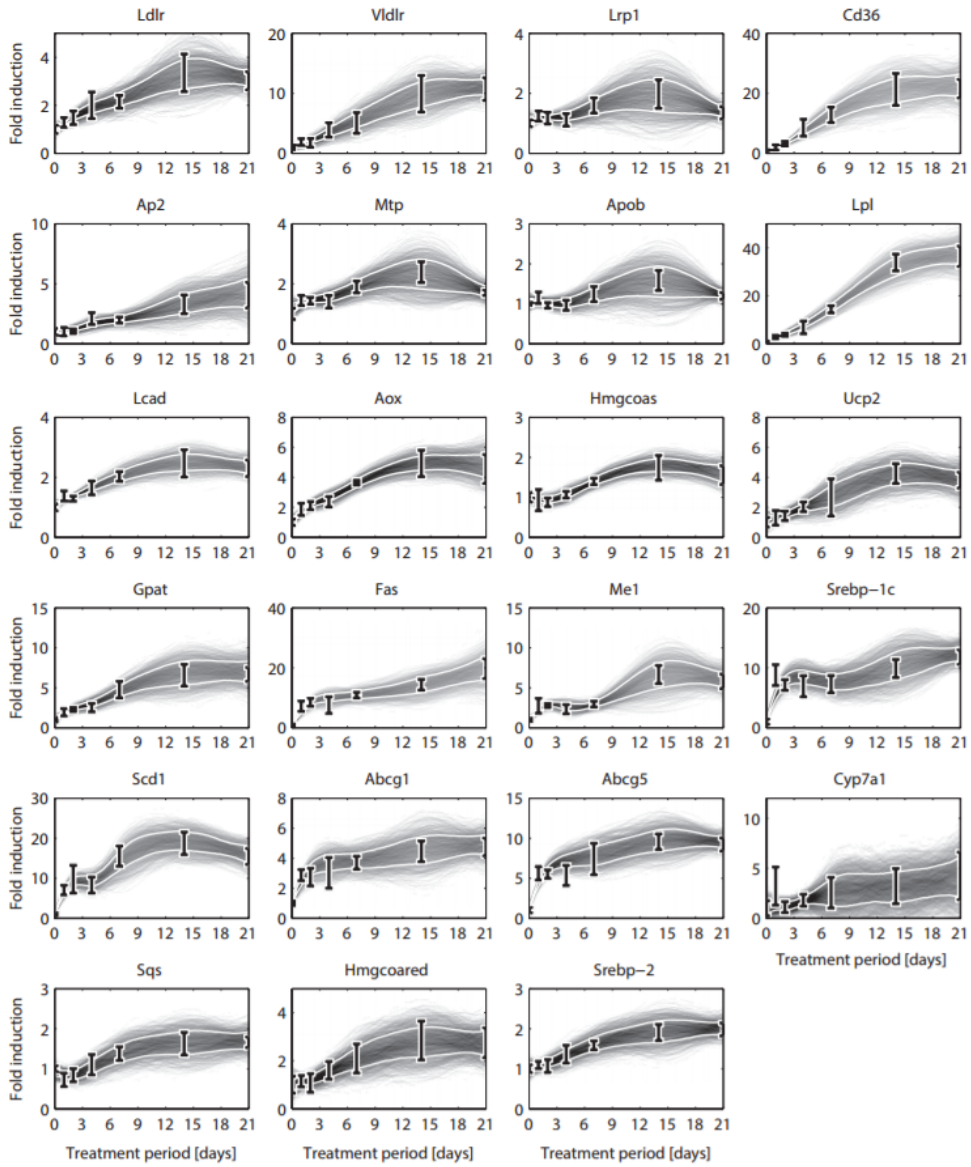

Figure B.2: Time-course data of relative hepatic gene expression levels.

Table B.3: Overview of the parameter-gene couples.

Parameter	Gene	Associated flux(es)
p_1	*Sqs*	f_1
p_1	*Hmgcoared*	f_1
p_1	*Srebp-2*	f_1
p_2	*Abcg1*	f_2
p_2	*Abcg5*	f_2
p_2	*Cyp7a1*	f_2
p_7	*Gpat*	f_7
p_7	*Fas*	f_7
p_7	*Me1*	f_7
p_7	*Srebp-1c*	f_7
p_7	*Scd1*	f_7
p_8	*Hmgcoa*	f_8, f_{25}
p_8	*Ucp2*	f_8, f_{25}
p_8	*Lcad*	f_8, f_{25}
p_8	*Aox*	f_8, f_{25}
p_{10}	*Gpat*	f_{10}
p_{10}	*Fas*	f_{10}
p_{10}	*Me1*	f_{10}
p_{10}	*Srebp-1c*	f_{10}
p_{10}	*Scd1*	f_{10}
p_{12}	*Cd36*	f_{12}
p_{12}	*Ap2*	f_{12}
p_{14}	*Mttp*	f_{14}, f_{15}
p_{15}	*Mttp*	f_{14}, f_{15}
p_{16}	*Ldlr*	f_{16}, f_{17}
p_{16}	*Vldlr*	f_{16}, f_{17}
p_{16}	*Lrp1*	f_{16}, f_{17}
p_{18}	*Lpl*	f_{22}
p_{22}	*ApoB*	f_{24}

Calculation of VLDL particle diameter

The following strategy was followed to calculate nascent VLDL particle diameters (D_{VLDL}). As each VLDL particle contains one apolipoprotein B particle, the number of TG and CE molecules per VLDL particle can be determined by correcting the specific lipid fluxes for the number of apolipoprotein B proteins. The core volume of a VLDL particle was subsequently determined assuming a molecular volume of 946.84 mL/mol for TG (TGmv) and a molecular volume of

685.48 ml/mol for CE (CEmv) [390]. A core radius (Rc) was calculated from the core volume assuming a spherical shape of the VLDL particles. Furthermore, the particle membrane accounts for an additional two nanometers (Rs) [391].

$$D_{VLDL} = 2(R_c + R_s)$$

$$R_c = \sqrt[3]{\frac{3V_c}{4\pi}}$$

$$V_c = 10^{21}\frac{TG_{cnt}TG_{mw} + CE_{cnt}CE_{mv}}{N_A}$$

$$TG_{cnt} = \frac{f_{14}}{f_{24}}$$

$$CE_{cnt} = \frac{f_{15}}{f_{24}}$$

Where NA is the constant of Avogadro.

Calculation of *de novo* lipogenesis

The fractional contribution of *de novo* lipogenesis was calculated as follows in the computational model:

$$FC_{DNL}(t) = \frac{[x_6](t) + [x_7](t)}{[x_4](t) + [x_5](t) + [x_6](t) = [x_7](t)}$$

Calculation of VLDL catabolic rate

VLDL catabolic rate was calculated as follows in the computational model:

$$CR_{VLDL}(t) = \frac{p_{16}(t) + p_{17}(t)}{p_{16}(t_0) + p_{17}(t_0)}$$

Calculation of cytoplasmic / ER TG concentration and production ratio

Equations for the ratio between cytoplasmic and ER TG concentration ($R_{cTGcyt,TGER}$) and production ($R_{pTGcyt,TGER}$) are given by:

$$R_{cTGcyt,TGer}(t) = \frac{[x_4](t) + [x_6](t)}{[x_5](t) + [x_7](t)}$$

$$R_{pTGcyt,TGer}(t) = \frac{f_7(t)}{f_{10}(t)}$$

Linking the computational model to experimental data

To enable the estimation of dynamic trajectories of metabolic parameters and fluxes, continuous dynamic descriptions of the experimental data were used as input for the computational approach. For this purpose, cubic smoothing splines were calculated that describe the dynamic trend of the experimental data. To account for experimental and biological uncertainties a collection of splines was calculated using a Monte Carlo approach. Different random samples of the experimental data were generated assuming Gaussian distributions with means and standard deviations of the data. Subsequently, for each generated sample a cubic smoothing spline was calculated. Measures of spread used for the Monte Carlo sampling of these quantities were estimated based on similar experiments that were performed [392]. An overview of the quantities that were experimentally observed and its relation to corresponding model components is presented in Table B.4. A model output y_i was coupled to experimental data d_i. Note that y_{13} to y_{15} were observed experimentally for the untreated phenotype only.

Table B.4: Overview of the quantities that were measured and their relation to corresponding model components.

Measurement	Model output	Equation
Hepatic TG	y_1	$[x_4]+[x_5]+[x_6]+[x_7]$
Hepatic CE	y_2	$[x_2]+[x_3]$
Hepatic free cholesterol	y_3	$[x_1]$
Plasma total cholesterol	y_4	$[x_9]+[x_{10}]$
HDL-cholesterol	y_5	$[x_{10}]$
Plasma TG	y_6	$[x_8]$
Plasma FFA	y_7	$[x_{11}]$
VLDL TG/C ratio	y_8	TG_{cnt}/CE_{cnt}
VLDL-diameter	y_9	D_{VLDL}
VLDL-TG production	y_{10}	f_{14}
VLDL catabolic rate	y_{11}	CR_{VLDL}
De novo lipogenesis	y_{12}	FC_{DNL}
Hepatic HDL-C uptake	y_{13}	f_{21}
Ratio cyt-TG / ER-TG concentration	y_{14}	$R_{cTGcyt,TGer}$
Ratio cyt-TG / ER-TG production	y_{15}	$R_{pTGcyt,TGer}$

Appendix C

Lipolytic enzymes in L-*G6pc*$^{+/+}$ and L-*G6pc*$^{-/-}$ mice

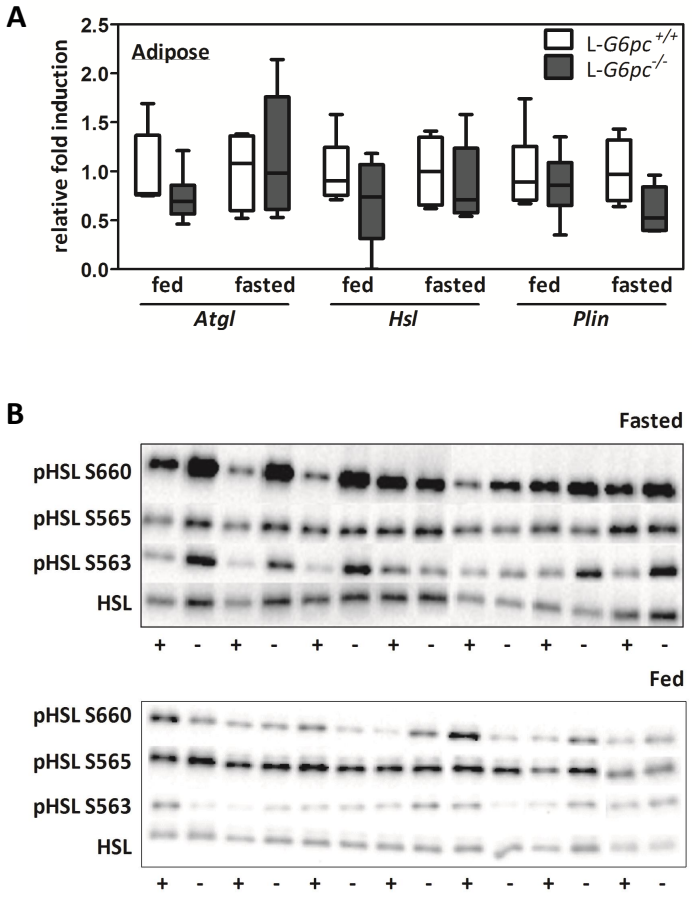

Figure C.1: A) Epididymal WAT relative mRNA fold induction of genes involved in lipolysis. B) Representative immunoblots for epididymal adipose tissue for indicated proteins, + lanes indicate L-*G6pc*$^{+/+}$ mice and lanes indicate L-*G6pc*$^{-/-}$ mice. See Figure 4.4D and 4.4E for quantification.